Journal of Ceramic Processing Research. Vol. 19, No. 3, pp. 243~248 (2018)

J O U R N A L O F
Ceramic Processing Research

Energy storage properties of dielectric $Bi_{1.5}Zn_{1.0}Nb_{1.5}O_7$ thick films on flexible metal foil substrates fabricated by aerosol deposition method

Jin-Woo Kim[a], Ji-Ho Lim[a], Seung-Hyun Kim[b], Chang Young Koo[c], Jungho Ryu[d,*] and Dae-Yong Jeong[a,*]

[a]*Department of Materials Science & Engineering, Inha University, Incheon 22212, Korea*
[b]*School of Engineering, Brown University, Providence, Rhode Island 02912, USA*
[c]*Quintess Co. Ltd., Incheon 21990, Korea*
[d]*School of Materials Science & Engineering, Yeungnam University, Gyeongsan, Gyeongbuk 38541, Korea*

In this study, we attempted to achieve a high energy density capacitor using nanocrystalline $Bi_{1.5}Zn_{1.0}Nb_{1.5}O_7$ (BZN) thick film, which is paraelectric material having a linear polarization-electric field behavior. Dense BZN thick films with thickness of 6~10 μm were deposited on the flexible metal substrates by Aerosol deposition. BZN thick films were annealed at various annealing conditions (400, 500 and 600 °C for 2 h) and their energy storage properties were characterized. The BZN films annealed at 400 °C showed the highest discharged energy density (8.87 J/cm^3) at 1400 kV/cm. The relative permittivity, which is measured with low electric field, was stable up to 250 °C, and the discharged energy density, which is measured with high electric field, was stable up to 125 °C.

Key words: Flexible substrate, Energy storage, BZN.

Introduction

With the recent development of wearable/portable electronic devices, it is required that the power sources should be flexible and miniaturized [1]. The embedded film capacitor is advantageous for miniaturization of electronic devices because they can reduce the space required for conventional passive components. In addition, using flexible metal foil or polymer as a substrate, it can be applied to wearable/portable electronic devices [2-4]. However, due to oxidation at high temperature or low glass transition temperature (T_g), flexible metal or polymer substrate has the restriction on the high temperature of processing and post annealing.

In general, high processing temperature is required to make dense ceramic, therefore the novel process has been developed for flexible devices [5-10]. Aerosol deposition (AD) is a physical method that can deposit a dense ceramic film at room temperature. In the process of fabricating the film, the ceramic powder injected through the nozzle strongly collides with the substrate with high kinetic energy and is broken into nano-size forming highly dense thick film at room temperature. Therefore, physically strong bonding between the substrate and the film is possible without post annealing [11], which is advantageous for the application of a flexible electronic devices [12] based on metal or polymer substrate. In addition, it is possible to deposit a dense film having nano-sized grains, which is hard to reach by conventional high temperature sintering method. However, since the crystallinity of the grains is greatly decreased by a strong physical collision, the post annealing process is often required to recover the dielectric properties through crystallization especially in ferroelectric dielectric materials [13, 14].

Ferroelectric materials, such as $Pb(Zr_{0.52},Ti_{0.48})O_3$ and $BaTiO_3$, are used as capacitors due to their high dielectric constant [15, 16]. However, since the high dielectric constant mainly obtainable at near the phase transition temperature, it is undesirable for a condition where wide range of workable temperature is required. In addition, because the post annealing process is required to enhance the crystallinity [17], it is difficult to apply it to a flexible substrate which cannot be subjected to a high temperature heat treatment [18]. In contrast, $Bi_{1.5}Zn_{1.0}Nb_{1.5}O_7$ (BZN), which is a paraelectric, has no phase transition above room temperature [19], and the relative permittivity changes with temperature variation is small [20]. Furthermore, BZN has a high relative permittivity of 150 or more can be achieved without post annealing. Therefore, it can be expected to be applied to embedded film capacitors and is easily applicable to flexible devices [2, 18]. In addition, since BZN is a paraelectric materials which has a linear polarization-electric field hysteresis, and relatively high dielectric breakdown strength [22], it can be applied to a pulsed power system with a high energy density capacitor for miniaturization of electronic devices.

*Corresponding author:
Tel : +82-32-860-7548
Fax: +82-32-862-5546
E-mail:dyjeong@inha.ac.kr

In previous studies, the dielectric properties of BZN AD films deposited on flexible polyimide substrates were characterized, but effect of post heat treatment could not be studied due to low T_g and T_m (melting temperature) of polyimide substrate [2]. In this study, BZN AD thick films were fabricated on flexible metal foil which is stable at relatively high temperature. The crystallinity and relative permittivity were measured with various annealing condition. Also, polarization-electric field hysteresis loops of BZN films and energy storage properties were characterized.

Experimental Procedure

The raw material powders of Bi_2O_3 (99.9% purity, Aldrich), ZnO (> 99% purity, Aldrich) and Nb_2O_5 (99.8% purity, NewTech Materials) were ball-milled for 24 hours at 400 rpm in ethanol solvent with zirconia balls. The uniformly mixed powders in the ethanol were completely dried for 24 hours in a convection oven at 80 ºC. The powders were calcined at 900 ºC for 2 hours in an electric furnace with a heating rate 10 ºC/min. To make BZN powders with adequate particle size for AD, the calcined BZN lumps were grounded by ball milling, dried and sieved.

BZN thick films were deposited on the flexible metal foil substrates using the aerosol deposition method. The flexible substrate is a 25 μm thick iron-chromium-nickel based alloy steel. The nozzle with 5 mm × 0.5 mm rectangular orifice was located 5 mm from the substrate. The BZN powders were injected through the nozzle with the nitrogen carrier gas. The injected BZN powders strongly collided with the substrate and the BZN thick films were deposited. The flow rate of the aerosol was controlled in 10~20 L/min through MFC (mass flow controller). The BZN thick films of 6~10 μm were prepared by controlling the number of repetitions. The prepared BZN thick films were annealed at 400, 500, and 600 ºC for 2 hours at a heating rate of 5 ºC/min.

The crystal structures of the BZN powders and the films were characterized by X-ray diffraction (HR-XRD, Philips X'pert pro MRD Diffractometer, Philips, Netherlands). To analyze the electrical characteristics of the BZN thick films, circular platinum upper electrodes with a diameter of 0.5 mm were deposited on the surface of the thick film by DC sputtering system. The relative permittivity and dielectric loss at 1, 10, 100, and 1000 kHz were measured by an impedance analyzer (Agilent Technologies 4194A, Santa Clara, CA). The polarization-electric field behaviors were measured at 100 Hz by P-E hysteresis loop (Precision multiferroic and ferroelectric test system, P-PMF-K; Radiant Technologies, Albuquerque, USA) and the energy storage characteristics of high voltage were calculated from P-E hysteresis loops. In the same way, the reliability and stability at high temperature were confirmed by measuring the relative permittivity, dielectric loss and polarization hysteresis loop at high temperature using a hot plate.

Result and Discussion

For the materials, BZN has slim and linear hysteretic behavior and its polarization is not saturated at high electric field, unlike ferroelectrics, thus it is advantageous in terms of high energy storage under high electric field [23]. BZN films were deposited on flexible metal foils by AD method because, the ceramic film deposited by the aerosol deposition method has a high dielectric constant due to the nano-sized crystalline and has a high dielectric breakdown strength due to a dense structure [24, 25].

Fig. 1 showed that the deposited BZN thick films retained the shape of the films without exfoliation when the substrate was bent.

As the metal substrate could stand up to 650 ºC without oxidation, we could anneal the BZN AD films to increase the crystallinity. Fig. 2 shows the X-ray

Fig. 1. A photo of the BZN thick film on the flexible metal foil substrate.

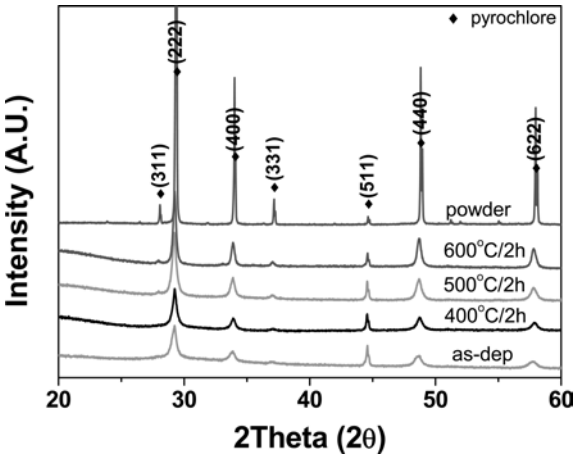

Fig. 2. X-ray diffraction patterns of powder and cubic pyrochlore BZN film on a flexible metal foil substrate under different annealing conditions.

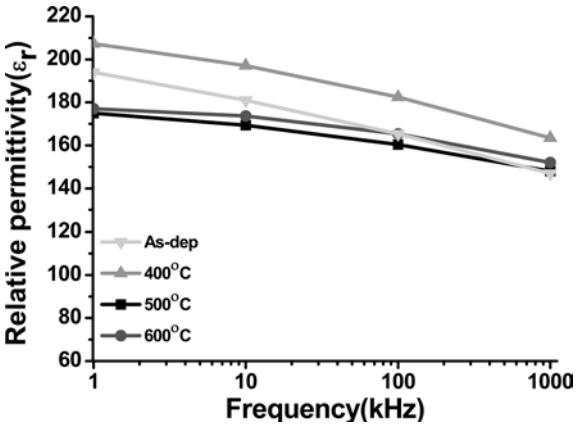

Fig. 3. Relative permittivity as a function of frequency for BZN film as-deposited, annealed at 400, 500, and 600 °C.

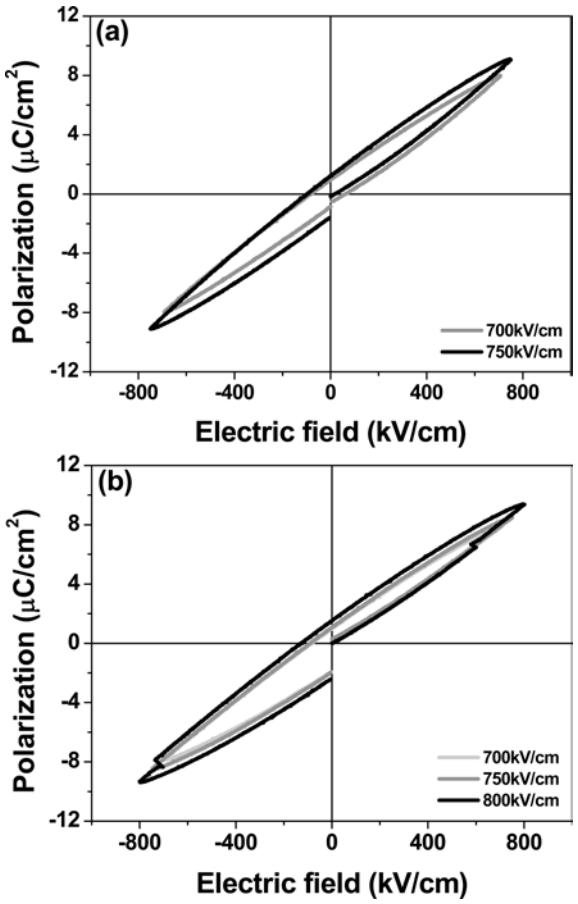

Fig. 4. Polarization-electric field behavior for (a) as-deposited and (b) annealed at 400 BZN films.

diffraction pattern of BZN powder and BZN thick films under various heat treatment conditions. BZN powder was synthesized in cubic pyrochlore phase without secondary phase. The intensity of diffraction peaks of as-deposited BZN thick film decreased compared to that of the powders because of the collision of the particles with high kinetic energy on the substrate [26]. The increased peak intensity of the annealed BZN films shows that the crystallinity of the films was increased by heat treatment temperature. In addition, it was confirmed that the full width at half maximum (FWHM) of the diffraction peak decreases with increasing the annealing temperature. According to the Scherrer equation, the FWHM of the diffraction peak is inversely proportional to the grain size [27]. The grain sizes calculated from the FWHM of (222) peaks in the XRD patterns were 18.04 nm for as-deposited, 21.77 nm for 400 °C annealed, 22.74 nm for 500 °C annealed and 31.10 nm for 600 °C annealed BZN AD films. The grain size of the BZN films increases with the increase of the annealing temperature.

The relative permittivity according to the annealing temperature is shown in fig. 3. The as-deposited BZN thick film has a relative permittivity of 194 at a frequency of 1 kHz. The relative permittivity of BZN film annealed at 400 °C increased to 207. For BZN films annealed at 500 and 600 °C, relative permittivity was lower than that of as-deposited BZN film and the values were 175 and 177, respectively. As mentioned above, the as-deposited BZN film has a high relative permittivity due to the nano-sized crystalline structure [18]. The BZN film annealed at 400 °C has an improved crystallinity during the annealing process, so the relative permittivity increased compared to the as-deposited BZN film. For the BZN films annealed at 500 and 600 °C, the grain size increases with the annealing temperature, so the relative permittivity close to the that of BZN bulk [19, 28].

Fig. 4(a) and (b) describes the P-E hysteresis loops at 100 Hz for the as-deposited and 400 °C annealed BZN thick films, respectively. As shown in fig. 4(a), when the 700 and 750 kV/cm electric field was applied, as-deposited BZN film showed a linear P-E hysteresis loop. Similarly, linear P-E hysteresis loops were shown up to 800 kV/cm for BZN film annealed at 400 °C in fig. 4 (b).

Fig. 5 (a) and (b) are the P-E hysteresis loops for the monopolar electrical cycling of as-deposited BZN film and BZN film annealed at 400 °C, respectively. The energy density of the capacitor is calculated from the P-E hysteresis loop by the following equation (1).

$$U = \int EdP \tag{1}$$

U is the density of the discharged energy, E is the electric field applied to the dielectric, and P is the magnitude of the polarization occurs in the dielectric by the electric field [29]. In addition, the energy loss (U_{loss}) due to joule heating is shown through the internal area of the P-E hysteresis loop. Therefore, in order to have a high energy density, the maximum polarization (P_{max}) and the dielectric breakdown strength (E_b) of the dielectric must be high. In addition, residual polarization (P_r) should be minimized to efficiently discharge the charged energy by reducing the energy loss [30]. The efficiency, which is an indicator of how efficiently the charged energy is

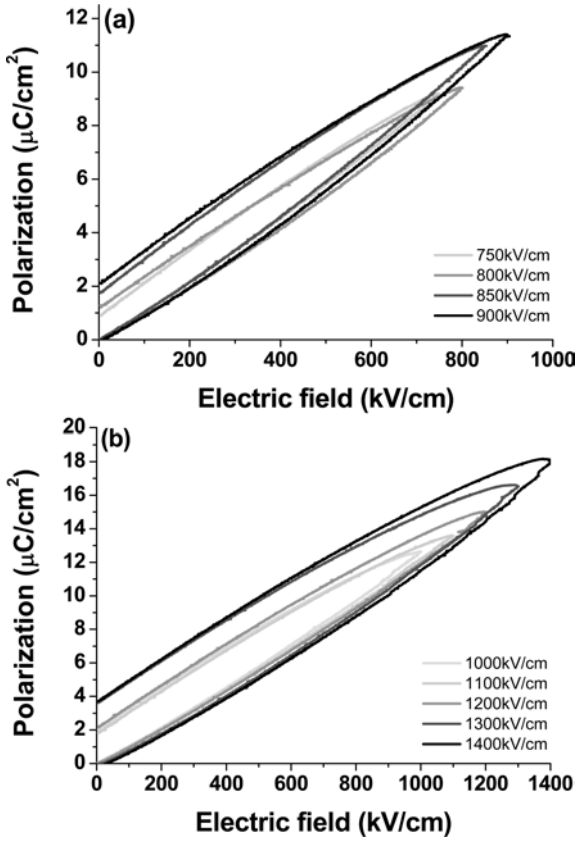

Fig. 5. Unipolar polarization-electric field behavior for BZN films (a) as-deposited and (b) annealed at 400 °C.

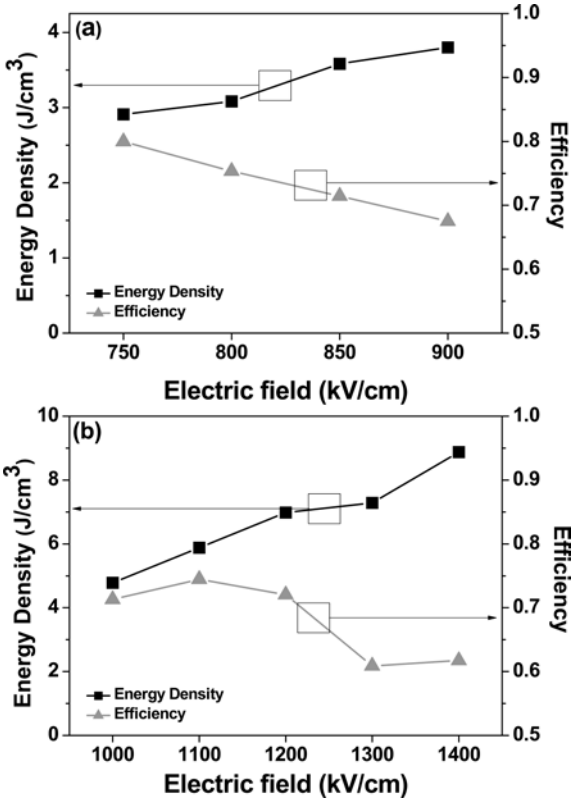

Fig. 6. Energy density and efficiency as a function of the electric field for (a) as deposited BZN film and (b) BZN film annealed at 400 °C.

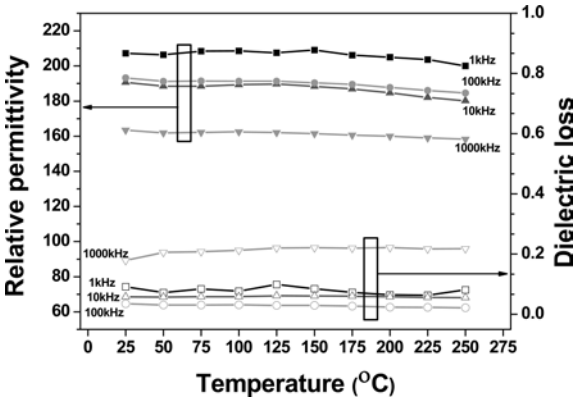

Fig. 7. Relative permittivity and dielectric loss as a function of temperature for BZN film annealed at 400 °C.

released, follows equation (2).

$$\eta = \frac{U}{U + U_{loss}} \tag{2}$$

U is the density of the discharged energy, $U + U_{loss}$ is the density of the charged energy, and η is the ratio of the discharged energy to the charged energy in the dielectric [29]. The maximum polarization (P_{max}) of both BZN films increased with the increase of the applied electric field. As-deposited BZN film of fig. 5 (a) showed a P_{max} of 11.15 μC/cm^2 at an electric field of 900 kV/cm. The BZN annealed at 400 °C in fig. 5 (b) showed a P_{max} of 18.15 μC/cm^2 at 1400 kV/cm. This indicates that the dielectric breakdown strength of the BZN annealed at 400 °C was significantly improved for monopolar electric cycling compared to the bipolar electric cycling in fig. 4(b).

The calculated energy density (U) and efficiency (η) were shown in fig. 6(a), (b) using the equation (1) and (2) based on the P-E hysteresis loops in fig. 5. As-deposited BZN depicted in fig. 6(a) showed an energy density of 2.91 J/cm^3 and an efficiency of 0.80 at 750 kV/cm, an energy density of 3.80 J/cm^3 and an efficiency of 0.67 at 900 kV/cm. BZN film annealed at 400 °C in fig. 6(b) showed the highest energy density of 8.87 J/cm^3 at 1400 kV/cm, but showed a low efficiency of 0.62. The maximum efficiency was 0.87 at 1000 kV/cm, with an energy density of 4.89 J/cm^3. As the applied electric field increases, the energy density increases, but the efficiency tends to decrease. It is because the P_{max} increases without saturation of polarization, but the width of the hysteresis loop widens with the increase of the applied electric field.

It is necessary to evaluate whether the capacitor can be used even at high temperature. When the capacitor used, cooling devices are used to lower the temperature of the heated capacitor and maintain performance. Since this cooling system also takes up a spatial volume in the

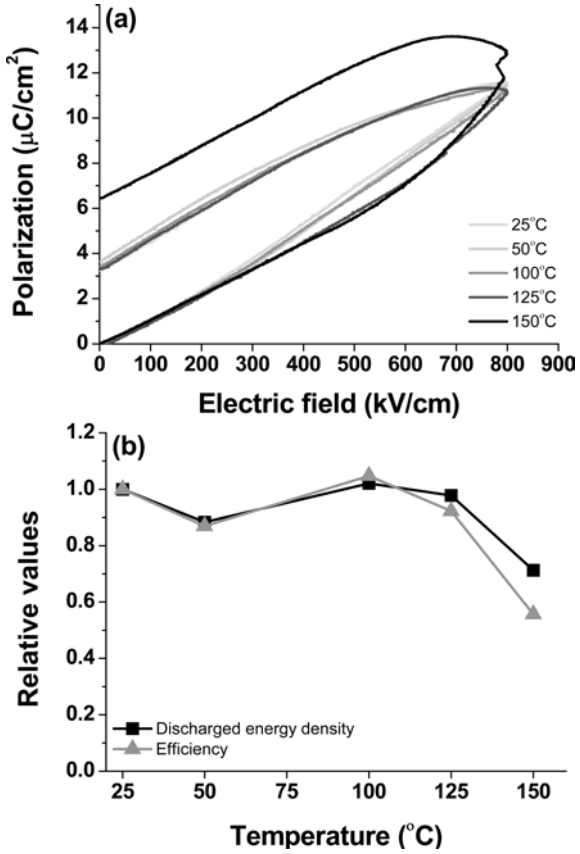

Fig. 8. (a) Unipolar P-E loops measured at 800 kV/cm in various temperature for BZN film annealed at 400 ºC and (b) relative values of energy density and efficiency at each temperature compared to 25 ºC from data in Fig. 8(a).

entire electrical system, it is advantageous for high energy density storage that the capacitor can operate at high temperature without cooling devices [31, 32]. Fig. 7 shows relative permittivity and dielectric loss with temperature variation for BZN film annealed at 400 ºC. The relative permittivity was 207 at room temperature, and 200 at 250 ºC for a frequency of 1 kHz. The average relative permittivity for each temperature was 206. Similarly, the dielectric loss at a room temperature of 1 kHz was 0.092, and 0.081 at 250 ºC. The average dielectric loss for each temperature was 0.079. Likewise, at 10, 100, 1000 kHz, it was confirmed that there was almost no change in relative permittivity and dielectric loss with temperature. Since BZN has no phase transition over a wide range of temperature, relative permittivity and dielectric loss hardly change [20]. Therefore, it is considered that dielectric properties of the 400 ºC annealed BZN film at low voltage is stable at the high temperature.

Fig. 8 presents the result of the P-E hysteresis loop, energy density and efficiency at high temperature. P-E hysteresis loops shown in fig. 8(a) were measured at 800 kV/cm. There is no significant change in the hysteresis loop up to 125 ºC, but P_r increased to 6.45 μC/cm^2 and width of the hysteresis wider at 150 ºC. The energy density and efficiency were calculated from the hysteresis in fig. 8(a) and compared with the values at room temperature. The relative energy density and efficiency were shown in fig. 8(b). When the energy density and the efficiency at room temperature were set to 1, the energy density and efficiency relative to the room temperature were 0.98 and 0.92 at 125 ºC. However, they were decreased to 0.71 and 0.56 at 150 ºC, respectively. That is, it can be seen that the energy storage properties were stable up to 125 ºC at a high electric field, but the stability and reliability were significantly reduced at 150 ºC.

Conclusions

In summary, BZN films were deposited on flexible metal substrates by AD at RT. The deposited BZN AD film was not exfoliated even under physical bending and maintained its shape. Due to the dense structure and the nano-sized grain, as-deposited and annealed at 400 ºC BZN films showed higher relative permittivity than 500 and 600 ºC. The as-deposited BZN film showed energy density of 3.80 J/cm^3 at 900 kV/cm. The BZN film annealed at 400 ºC exhibited higher dielectric breakdown strength (1400 kV/cm) and energy density more than twice that of as-deposited one (8.87 J/cm^3). Since there is no phase transition in that temperature range, there is almost no change in the relative permittivity and dielectric loss up to 250 ºC. Also, because the difference of energy storage density and efficiency were not large in a temperature range of 25 to 125 ºC, it can be said that those at high electric field are stable at high temperature.

Acknowledgments

This study was supported by the National Research Foundation of Korea (Grant No: 2017K1A4A3013662).

References

1. Z. Gao, Y. Zhang, N. Song and X. Li, Electrochim. Acta, 246[57] (2017) 507-516.
2. J. Ryu, K.-Y. Kim, J.-J. Choi, B.-D. Hahn, W.-H Yoon, B.-K. Lee, D.-S. Park, D.-Y. Jeong and C. Park, J. Am. Ceram. Soc. 92[2] (2009) 524-527.
3. B. Laughlin, J. F. Ihlefeld, P. Daniels and J.-P. Maria, Thin Solid Films 516[10] (2008) 3294-3297.
4. A. I. Kingon and S. Srinivasan, Nat. Mater. 4 (2005) 233-237.
5. J.-F. Li, K. Wang, B.-P. Zhang and L.-M. Zhang, J. Am. Ceram. Soc. 89[2] (2006) 706-709.
6. Y. Zhen, J.-F. Li, K. Wang, Y. Yan and L. Yu, Mater. Sci. Eng. B 176[14] (2011) 1110-1114.
7. F. M. Pontes, E. R. Leite, E. Longo, J. A. Varela, E. B. Araujo and J. A. Eiras, Appl. Phys. Lett. 76[17] (2000) 2433-2435.
8. A. Biswas, H. Park and W. M. Sigmund, Ceram. Int. 38[1]

(2012) 883-886.
9. J.-I. Park, G.-Y. Lee, J. Yang, C.-S. Kim and S.-H. Ahn, J. Compos. Mater. 50[12] (2015) 1573-1579.
10. G.-T. Hwang, J. Yang, S. H. Yang, H.-Y. Lee, M. Lee, D. Y. Park, J. H. Han, S. J. Lee, C. K. Jeong, J. Kim, K.-I. Park and K. J. Lee, Adv. Energy Mater. 5[10] (2015) 1500051 1-8.
11. J. Akedo and M. Lebedev, Jpn. J. Appl. Phys. 40[9B] (2001) 5528-5532.
12. X. Cai, M. Peng, X. Yu, Y. Fu and D. Zou, J. Mater. Chem. C 2[7] (2014) 1184-1200.
13. Y. Imanaka, N. Hayashi, M. Takenouchi, and J. Akedo, J. Eur. Ceram. Soc. 27[8-9] (2007) 2789-2795.
14. J. Ryu, J.-J. Choi, B.-D. Hahn, D.-S. Park, W.-H Yoon and K.-H. Kim, Appl. Phys. Lett. 90[15] (2007) 152901-1-3.
15. M.D. Nguyen, M. Dekkers, E. Houwman, R. Steenwelle and X. Wan, Appl. Phys. Lett. 99[25] (2011) 252904-1-4.
16. Y. Tan, J. Zhang, Y. Wu, C. Wang, V. Koval, B. Shi, H. Ye, R. McKinnon, G. Viola and H. Yan, Sci. Rep. 5 (2015) 9953 1-9.
17. H. Tsuda, M. Nakada, J. Akedo and K. Ohashi, IEEE Trans. Ultrason., Ferroelect., Freq. Contr. 55[5] (2008) 975-979.
18. J. Ryu, K.-Y. Kim, J.-J. Choi, B.-D. Hahn, W.-H Yoon, D.-S. Park and C. Park, J. Am. Ceram. Soc. 91[10] (2008) 3399-3401.
19. S. Kamba, V. Porokhonskyy, A. Pashkin, V. Bovtun, J. Petzelt, J. C. Nino, S. Trolier-Mckinstry, M. T. Lanagan and C. A. Randall, Phys. Rev. B 66[5] (2002) 054106-1-8.
20. X. Wang, H. Wang and X. Yao, J. Am. Cera. Soc. 80[10] (1997) 2745-2748.
21. W. Ren, S. Trolier-McKinstry, C. A. Randall and T. R. Shrout, J. Appl. Phys. 89[1] (2001) 767-774.
22. E. K. Michael and S. Trolier-McKinstry, J. Am. Ceram. Soc. 98[4] (2015) 1223-1229.
23. C. Linder and C. Miehe, J. Mech, Phys. Solids 60[5] (2012) 882-903.
24. S.-B. Kang, H.S. Kim, J.G. Lee, C.-K. Park, J. Ryu, J.-J. Choi, B.-D. Hahn, L. Wang and D.-Y. Jeong, Ceram. Int. 42[1B] (2016) 1740-1745.
25. S.-B. Kang, M.-G. Choi, D.-Y. Jeong, Y.-M. Kong and J. Ryu, IEEE Trans. Dielectr. eletr. Insul. 22[3] (2016) 1740-1745.
26. J.-J. Choi, J.-H. Jang, B.-D. Hahn, D.-S. Park, W.-H. Yoon, J. Ryu and C. Park J. Am. Ceram. Soc. 90[11] (2007) 3389-3394.
27. A. K. Zak, W.H. A. Majid, M.E. Abrishami and R. Yousefi, Solid State Sci. 13[1] (2011) 251-256.
28. M. Valant and P. K. Davies, J. Am. Ceram. Soc. 83[1] (2000) 147-153.
29. Q. Chen, Y. Wang, X. Zhou, Q.M. Zhang and S. Zhang, Appl. Phys. Lett. 92[12] (2008) 142909-1-3.
30. B. Chu, X. Zhou, K. Ren, B. Neese, M. Lin, Q. Wang, F. Bauer and Q.M. Zhang, Science 313[5785] (2006) 334-336.
31. Q. Li, L. Chen, M.R. Gadinski, S. Zhang, G. Zhang, H. U. Li, E. Iagodkine, A. Haque, L.-Q. Chen, T. N. Jackson and Q. Wang, nature 523 (2015) 576-579.
32. U. Balachandran, M. Narayanan, S. Liu and B. Ma, Jpn. J. App. Phys. 52[5S1] (2013) 05DA10-1-4.